Journal of
Synchrotron
Radiation

ISSN 0909-0495

Received 15 April 2005
Accepted 23 June 2005

The effect of pressure on the crystal structure of hexagonal L-cystine

Stephen A. Moggach,[a] David R. Allan,[a] Simon Parsons,[a]* Lindsay Sawyer[b] and John E. Warren[c]

[a]School of Chemistry and Centre for Science at Extreme Conditions, The University of Edinburgh, King's Buildings, West Mains Road, Edinburgh EH9 3JJ, UK, [b]School of Biological Sciences and Centre for Science at Extreme Conditions, The University of Edinburgh, King's Buildings, Mayfield Road, Edinburgh EH9 3JR, UK, and [c]CCLRC Daresbury Laboratory, Warrington WA4 4AD, UK. E-mail: s.parsons@ed.ac.uk

The crystal structure of hexagonal L-cystine has been determined at room temperature at pressures between 0.4 and 3.7 GPa; unit-cell dimensions were measured up to 6.4 GPa. The structure of this phase consists of molecules in their zwitterionic form, and crystallizes in the hexagonal space group $P6_122$. The structure consists of hydrogen-bonded layers which are strongly reminiscent of those seen in α-glycine, and consist of $R_4^4(16)$ hydrogen-bonded ring motifs. These layers are connected on one side by the disulfide bridges within the cystine molecules, and on the other by NH$\cdots$O hydrogen bonds to other glycine-like layers. The most compressible unit-cell dimension, and the direction of greatest strain in the structure, is along the *c*-axis, and application of pressure pushes the layers closer together. The compression occurs approximately equally in the regions of the interlayer hydrogen bonds and the disulfide bridges; in the latter, changes in the C—S—S—C torsion angles allow the cystine molecules to act like springs. The effects of pressure can be interpreted in terms of closing-up of voids in the structure, and this leads to (i) a lessening of the N—C—C—O and C—S—S—C torsional angles, (ii) shortening of the N—H$\cdots$O hydrogen bonds by 0.10–0.60 Å and (iii) a further shortening of an already short S$\cdots$S contact from 3.444 (4) Å to 3.264 (4) Å.

Keywords: amino acid; hydrogen bonding; high-pressure single-crystal diffraction.

1. Introduction

The application of pressure is becoming an ever-more popular technique with which to analyse the nature of intermolecular interactions [for example, Oswald, Allan, Motherwell & Parsons (2005), Oswald, Allan, Day, Motherwell & Parsons (2005), Wunschel *et al.* (2003), Boldyreva (2004*a*,*b*), Allan *et al.* (1999, 2001)]. Application of pressure (up to $\sim$10 GPa, approximately 10^5 atm) to non-cubic organic crystals commonly results in the anisotropic closure of voids in the structure along with an increase in the number and strength of weak interactions, such as CH$\cdots$O hydrogen bonds. In some cases the discovery of new phases of materials is observed with increasing pressure (Moggach *et al.*, 2005). In α-amino acids the compression of numerous weak CH$\cdots$O interactions may be extremely important, as they have a supporting role to medium-strength hydrogen bonds under ambient pressure conditions, *e.g.* NH$\cdots$O (Desiraju & Steiner, 1999; Derewenda *et al.*, 1995). The compression of such interactions has been discussed in other studies, such as the compression of L-serine-I (Moggach *et al.*, 2005).

Most molecular systems that have been studied previously are relatively simple with small unit cells with volumes ranging from a few hundred up to a few thousand Å^3. In this study the effect of pressure on hexagonal L-cystine (I) was studied on station 9.8 at the CCLRC Daresbury Laboratory (Cernik *et al.*, 1997) as part of our on-going research of the effect of pressure on amino acids and related compounds. Although L-cystine is a moderately small organic molecule containing 14 non-H atoms, it crystallizes in a high symmetry space group ($P6_122$), with an unusually long axis (c = 55.9 Å). Attempts to study the compound at high pressure in the home laboratory were frustrated by difficulties in resolving data along c^*. The low divergence of synchrotron radiation, however, enabled this difficulty to be overcome, and we report here a compression study of L-cystine carried out using the high-pressure facilities on station 9.8 at SRS Daresbury Laboratory. Structural data to 3.7 GPa, and unit-cell dimensions up to 6.4 GPa, are reported.

L-Cystine is a dimer of L-cysteine produced by oxidation of the side-chain thiols to form the so-called disulfide bridge. The disulfide bridge is a structurally important feature in proteins, being the only common covalent linkage to occur within and

between polypeptide chains. Naturally occurring disulphide bridges are found in many proteins that are secreted by cells where their presence adds stability to the generally fragile protein structure. Common examples include the defensive immunoglobulin proteins, the hydrolytic enzymes like trypsin and lysozyme, and structural proteins like keratin. Analyses of the conformations adopted by cystine (Thornton, 1981; Richardson, 1981; Morris *et al.*, 1992; Görbitz, 1990) reveals that left- (−C−S−S−C− = $\chi3 = -90^\circ$) and right-handed disulphides are equally distributed in globular proteins. The distributions of the $\chi1$ and $\chi2$ angles are also more or less as expected. $\chi1$ favours the -60° conformation since there is less crowding between the S and the adjacent peptide carbonyl; $\chi2$ tends to adopt a value of around -85°. A more recent analysis, including that of the disulphide bridge environment by Bhattacharaya *et al.* (2004), confirms and extends these results using data from 1266 polypeptide chains in the Protein Data Bank (Berman *et al.*, 2000) with *R*-factors $\leq 20\%$ and data resolution ≤ 2 Å. It includes an analysis of the S to main-chain (carbonyl) oxygen distances that determines the average distance to be 3.6 (2) Å, about a quarter of which are interactions with their own carbonyl oxygen.

2. Experimental

2.1. Crystal growth

All starting materials were purchased from Sigma-Aldrich and used as received. L-Cystine (1.48 g, 6.16 mmol) was dissolved in warm ammonium hydroxide solution (ACS reagent, NH_3 28.0–30.0%, 8 cm^3) and crystallized on cooling to ambient temperature (Dahaoui *et al.*, 1999). A high-quality hexagonally shaped crystal of dimensions 0.1 mm × 0.2 mm × 0.2 mm was then loaded into a Merrill–Bassett diamond anvil cell (DAC; Merrill & Bassett, 1974).

2.2. High-pressure crystallography

2.2.1. General procedures. High-pressure experiments were carried out with a Merrill–Bassett DAC equipped with 600 µm culet-cut diamonds and a tungsten gasket. The sample and a chip of ruby (as a pressure calibrant) were loaded into the DAC with a 1:1 mixture of pentane and isopentane as a hydrostatic medium. The ruby fluorescence method was utilized to measure the pressure (Piermarini *et al.*, 1975).

2.2.2. Data collection, reduction and refinement. A sphere of data was collected on a crystal of L-cystine at ambient temperature and pressure in order to provide data for comparison with the high-pressure studies, which were also performed at ambient temperature (see below). Diffraction data were collected on a single crystal of L-cystine on a Bruker SMART APEX diffractometer with graphite-monochromated Mo $K\alpha$ radiation ($\lambda = 0.71073$ Å). These data were integrated using the program *SAINT* (Bruker-AXS, 2003), while the absorption correction was carried out using the program *SADABS* (Sheldrick, 2004). Refinement was carried out against $|F|^2$ using all data (*CRYSTALS*; Betteridge *et al.*, 2003) starting from the low-temperature (110 K) coordinates of Dahaoui *et al.* (1999). The final conventional *R*-factor was 0.0476 for 898 data. Listings of crystal and refinement data are given in Table 1.[1]

High-pressure diffraction data were collected with synchrotron radiation on a Bruker APEX II diffractometer at the CCLRC Daresbury Laboratory on station 9.8 ($\lambda = 0.6774$ Å); see below. Data were collected in ω-scans in eight settings of 2θ and φ with a frame and step size of 1 s and 0.2°, respectively. This data collection strategy was based on that described by Dawson *et al.* (2004). The data were integrated using the program *SAINT* using 'dynamic masks' to avoid integration of regions of the detector shaded by the body of the pressure cell (Dawson *et al.*, 2004). Additional masks were also added to mask out the three most intense powder rings (100, 002 and 101) from the beryllium backing discs. This additional mask was required because the low divergence of synchrotron radiation gave the beryllium powder pattern a much more textured spotty appearance than if collected using a sealed-tube laboratory X-ray source. Application of this additional mask removed the possibility of unreliable measurements of sample reflections which coincided with the beryllium rings and was shown to improve the merging statistics slightly. Absorption corrections for the DAC and sample were carried out using the programs *SHADE* (Parsons, 2004) and *SADABS*, respectively. Data collections were taken in approximately 1.0 GPa steps from 0.4 GPa up to a final pressure of 6.4 GPa.

Refinements of L-cystine were carried out starting from the published low-temperature coordinates (Dahaoui *et al.*, 1999). Refinements were carried out against $|F|^2$ using all data (*CRYSTALS*). Because of the low completeness of the data sets, all 1,2 and 1,3 distances were restrained to the values observed in the ambient pressure structure. Specifically, the applied restraints were as follows: distances (Å) S1—C1 1.818 (20); C3—O2 1.267 (20); C3—O1 1.245 (20); C3—C2 1.538 (20); C2—N1 1.480 (20); C2—C1 1.523 (20); angles (°) O1—C3—O2 125.73 (100); O1—C3—C2 117.25 (100); O2—C3—C2 117.01 (100); N1—C2—C1 112.05 (100); N1—C2—C3 109.67 (100); C1—C2—C3 113.39 (100). H atoms attached to carbon and nitrogen were placed geometrically and not refined. The numbering scheme used is the same as Cambridge Structural Database (CSD) refcode LCYSTI14 (Dahaoui *et al.*, 1999).

All non-H atoms were refined with anisotropic displacement parameters to 2.3 GPa. At 3.7 GPa only the S atoms were refined anisotropically, while all other non-H atoms were refined with isotropic displacement parameters. This parameterization strategy was dictated by the quality of the data collected: reflections broadened with increasing pressure, making indexing and integration increasingly difficult. Acceptable refinements could be obtained for the final 5.0 and 6.4 GPa data sets; unit-cell dimensions at these pressures were $a = 5.21970$ (10), $c = 52.793$ (6) Å and $a = 5.1852$ (3), $c =$

[1] Supplementary data for this paper are available from the IUCr electronic archives (Reference: XD5007). Services for accessing these data are described at the back of the journal.

Table 1
Crystallographic data for hexagonal L-cystine at ambient temperature and pressure, and at increasing pressures.

	Pressure (GPa)				
	0	0.4	1.4	2.3	3.7
Crystal data					
Chemical formula	$C_6H_{12}N_2O_4S_2$	$C_6H_{12}N_2O_4S_2$	$C_6H_{12}N_2O_4S_2$	$C_6H_{12}N_2O_4S_2$	$C_6H_{12}N_2O_4S_2$
M_r	240.30	240.30	240.30	240.30	240.30
Cell setting, space group	Hexagonal, $P6_122$	Hexagonal, $P6_122$	Hexagonal, $P6_122$	Hexagonal, $P6_122$	Hexagonal, $P6_122$
a, c (Å)	5.4203 (5), 55.980 (12)	5.4030 (1), 55.984 (4)	5.3524 (2), 55.087 (14)	5.3141 (1), 54.291 (3)	5.26630 (10), 53.549 (5)
V (Å^3)	1424.3 (4)	1415.40 (10)	1366.7 (4)	1327.75 (8)	1286.17 (13)
Z	6	6	6	6	6
D_x (Mg m^{-3})	1.681	1.691	1.752	1.803	1.861
Radiation type	Mo $K\alpha$	Synchrotron	Synchrotron	Synchrotron	Synchrotron
No. of reflections for cell parameters	1792	3156	1652	3365	3341
θ range (°)	9–46	9–54	9–53	9–53	9–51
μ (mm^{-1})	0.55	0.56	0.57	0.59	0.61
Temperature (K)	293	293	293	293	293
Crystal form, colour	Hexagonal block, colourless	Hexagonal block, colourless	Hexagonal block, colourless	Hexagonal block, colourless	Hexagonal block, colourless
Crystal size (mm)	0.32 × 0.17 × 0.15	0.20 × 0.20 × 0.10	0.20 × 0.20 × 0.10	0.20 × 0.20 × 0.10	0.20 × 0.20 × 0.10
Data collection					
Diffractometer	Bruker APEX	Bruker APEX II	Bruker APEX II	Bruker APEX II	Bruker APEX II
Data collection method	ω	ω	ω	ω	ω
Absorption correction	Multi-scan (based on symmetry-related measurements)	Multi-scan (based on symmetry-related measurements)	Multi-scan (based on symmetry-related measurements)	Multi-scan (based on symmetry-related measurements)	Multi-scan (based on symmetry-related measurements)
T_{min}	0.81	0.71	0.62	0.64	0.56
T_{max}	0.92	0.95	0.94	0.94	0.94
No. of measured, independent and observed parameters	16236, 965, 898	4719, 539, 490	4645, 492, 464	4229, 492, 438	4229, 467, 439
Criterion for observed reflections	$I > 2.00\,u(I)$	$I > 2.00\,u(I)$	$I > 2.00\,u(I)$	$I > 2.00\,u(I)$	$I > 2.00\,u(I)$
Completeness (%)	99.0	45.4	45.5	45.5	45.9
R_{int}	0.085	0.047	0.047	0.053	0.063
θ_{max} (°)	26.4	28.5	28.1	28.1	27.9
Range of h, k, l	$-6 \rightarrow h \rightarrow 6$ $-6 \rightarrow k \rightarrow 6$ $-64 \rightarrow l \rightarrow 68$	$-7 \rightarrow h \rightarrow 7$ $-7 \rightarrow k \rightarrow 6$ $-29 \rightarrow l \rightarrow 29$	$-6 \rightarrow h \rightarrow 6$ $-7 \rightarrow k \rightarrow 7$ $-28 \rightarrow l \rightarrow 28$	$-7 \rightarrow h \rightarrow 6$ $-7 \rightarrow k \rightarrow 6$ $-28 \rightarrow l \rightarrow 28$	$-6 \rightarrow h \rightarrow 6$ $-6 \rightarrow k \rightarrow 6$ $-28 \rightarrow l \rightarrow 28$
Refinement					
Refinement on	F^2	F^2	F^2	F^2	F^2
$R[F^2 > 2\sigma(F^2)]$, $wR(F^2)$, S	0.048, 0.105, 1.07	0.035, 0.089, 1.06	0.036, 0.089, 1.05	0.048, 0.112, 1.05	0.093, 0.214, 1.09
No. of reflections	956	513	485	458	451
No. of parameters	64	64	64	64	34
H-atom treatment	Not refined	Not refined	Not refined	Not refined	Not refined
Weighting scheme	Calculated $w = 1/[\sigma^2(F^2) + 0.03 + 3.29P]$ where $P = [\max(F_o^2,0) + 2F_c^2]/3$	Calculated $w = 1/[\sigma^2(F^2) + 0.05 + 0.8P]$ where $P = [\max(F_o^2,0) + 2F_c^2]/3$	Calculated $w = 1/[\sigma^2(F^2) + 0.05 + 1.06P]$ where $P = [\max(F_o^2,0) + 2F_c^2]/3$	Calculated $w = 1/[\sigma^2(F^2) + 0.03 + 3.33P]$ where $P = [\max(F_o^2,0) + 2F_c^2]/3$	Calculated $w = 1/[\sigma^2(F^2) + 0.00 + 18.85P]$ where $P = [\max(F_o^2,0) + 2F_c^2]/3$
$(\Delta/\sigma)_{max}$	0.001	<0.0001	<0.0001	<0.0001	<0.0001
$\Delta\rho_{max}$, $\Delta\rho_{min}$ (e Å^{-3})	0.35, −0.35	0.14, −0.19	0.22, −0.17	0.27, −0.21	0.54, −0.60

52.172 (7) Å, respectively. The deterioration of the data quality was the result of increasing mosaic spread with increasing pressure, a frequent problem with crystallographic pressure studies on soft materials. Listings of crystal and refinement data are given in Table 1.

2.2.3. High-pressure data collection on station 9.8, SRS, Daresbury Laboratory. High-pressure single-crystal diffraction experiments may be carried out at SRS, Daresbury Laboratory on stations 9.8 and 16.2SMX. Both facilities are equipped with Bruker D8 three-circle fixed-χ goniometers with APEXII detectors. On most currently available models of home-laboratory X-ray diffractometer it is necessary to re-machine the collimator and beam stop in order that full φ-rotations may be performed. This is not necessary on a synchrotron beamline because the fixed distance constraints of tube-to-collimator housing are absent. In 'high-pressure mode' at the SRS the collimator is retracted towards the X-ray source by 30 mm into the space where the tube housing and optics would usually sit. This increases the collimator-to-sample distance to allow full 360° rotation in φ; rotations in ω are restricted only by the position of the detector. The distance from sample to beam stop a custom beam was set at

70 mm. Alignment procedures follow Dawson *et al.* (2004). We have found that the ease and simplicity of set-up combined with small beam divergence and high brightness allows high pressure to be a routine option for users of the facilities at the SRS.

2.2.4. Software for structure analysis. Crystal structures were visualized using the programs *CAMERON* (Watkin *et al.*, 1993), *DIAMOND* (Crystal Impact, 2004), *MERCURY* (Bruno *et al.*, 2002) and *XP* (Sheldrick, 1997). Analyses were carried out using *PLATON* (Spek, 2004), as incorporated in the *WIN-GX* suite (Farrugia, 1999). Searches of the CSD (Allen, 2002; Allen & Motherwell, 2002) were performed using the program *CONQUEST* and version 5.26 of the database with updates up to November 2004.

Topological calculations of void distributions were carried out using *TOPOS* (Blatov *et al.*, 2000; Blatov & Shevchenko, 2003). Considerable simplification of the void distributions can be gained by clustering; voids were therefore clustered using what the program calls the 'floating' method with the 'size' parameter specified as 1.0.

Equation-of-state calculations were carried out using *EOSFIT* (Angel, 2002).

3. Results

3.1. The structure of hexagonal L-cystine at ambient pressure

L-Cystine crystallizes in two polymorphic forms: a tetragonal phase ($P4_1$) that was characterized by Chaney & Steinrauf (1974) and a hexagonal phase ($P6_122$) first investigated by Oughton & Harrison (1959) but more recently in a charge density study by Dahaoui *et al.* (1999). We have redetermined the structure at room temperature (Fig. 1) in order to be able to compare all structures obtained here under similar conditions of temperature. Though we quote our own room-temperature structural parameters, our interpretation of the structure owes much to the paper of Dahaoui *et al.* (1999), which, in addition to describing the structure of cystine at high resolution, also contains a database survey of geometries and interactions of crystal structures containing —CSSC— moieties.

Both the tetragonal and hexagonal phases of L-cystine crystallize with the molecule in its zwitterionic form. The S—S bond distances in the two polymorphs [2.042 (6) and 2.043 (2) Å, respectively] do not differ significantly from the average for such bonds in the CSD [2.039 (2) Å]. The same comment applies to the C—S—S—C torsion angle, which is positive in both forms [69.3 (2)° and 75.18 (5)°, respectively]. The hydrochloride and hydrobromide salts of L-cystine have both been structurally characterized in the anhydrous forms and as dehydrates; interestingly, these all have negative C—S—S—C torsion angles in the range −79° to −83°. The length of S—S bonds in compounds containing C—S—S—C moieties has been shown to be dependent on the torsion angle about the S—S bond: torsion angles which approach 90° result in short S—S bonds because π-interactions are optimized and repulsions between S-based lone pairs are minimized

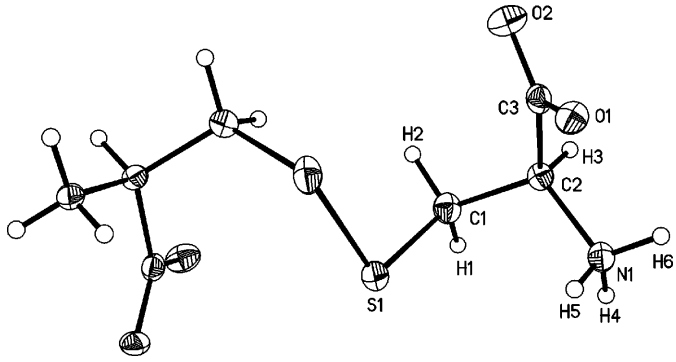

Figure 1
The molecular structure of L-cystine at ambient temperature and pressure showing atom labelling. Ellipsoids are drawn at the 30% probability level, and H atoms are shown as spheres of arbitrary radius.

(Dahaoui *et al.*, 1999). The values of $\chi1$ and $\chi2$ (*i.e.* the torsion angles N1—C2—C1—S1 and C2—C1—S1—S1′) are 56.1 (5)° and 80.1 (3)°, respectively; these values are relatively less common in proteins (see *Introduction*).

In this study the effect of pressure on the crystal structure of the hexagonal phase was studied. The principal intermolecular interactions take the form of unusually short S···S contacts and NH···O hydrogen bonds, formed between the ammonium and carboxylate moieties. The NH···O hydrogen bonds lead to the formation of layers which lie perpendicular to the *c*-axis. The layers can be considered to be formed from the intersection of two primary *C*(5) chain motifs (Bernstein *et al.*, 1995), one *via* N1—H4···O1 interactions, the other *via* N1—H5···O2 interactions (Fig. 2*a*). The first of these interactions is substantially bifurcated (Jeffrey & Maluszynska, 1982) with donor-to-acceptor distances (*i.e.* N···O) in N1—H4···O1/O2 measuring 2.792 (5)/3.147 (5) Å.

The structure of the layers is strongly reminiscent of layers formed perpendicular to the *b*-axis in α-glycine (Fig. 2*b*; Boldyreva *et al.*, 2003). In both cases intersection of the *C*(5) chains leads to formation of a secondary-level $R_4^4(16)$ ring motif. In the asymmetric unit of LCYSTI14, and all the structures reported here, the chains based on N1—H4···O1 and N1—H5···O2 interactions are respectively formed along lattice repeats in the [010] and [110] directions, but these directions interchange for successive layers generated by the 6_1 screw axis. Head-to-tail NH···OOC motifs are often observed in amino acid structures and are usually associated with a cell dimension of ∼5.5 Å. This is also observed in L-cystine with an *a*-axis length of 5.4203 (5) Å.

The hydrogen-bonded layers are linked to other such layers on one side by covalent S—S bridges and on the other by NH···O hydrogen bonds (Fig. 3). The latter are formed *via* N1—H6···O1 interactions, which connect pairs of molecules in successive layers, forming an $R_2^2(10)$ ring motif (Fig. 4).

Weak CH···O hydrogen bonds are also present at ambient pressure and can play an important role in stabilizing medium-strength hydrogen bonds, *e.g.* NH···O (Desiraju & Steiner, 1999; Derewenda *et al.*, 1995). Under ambient pressure two such interactions are present, both of which occur within the glycine-like layers already described. The first of these, C1—

H1···O2, runs approximately parallel to N1—H4···O1 and bisects the $R_4^4(16)$ ring motif described above, while the second, C2—H3···O1, runs in the same direction as N1—H5···O2. If all other hydrogen-bonding interactions are ignored, these weak C—H···O interactions combine to produce an $R_4^4(16)$ ring motif of their own (Fig. 2*c*).

At ambient pressure, S···S intermolecular interactions are formed (Fig. 3); the S···S distance [3.444 (4) Å] is much shorter than the sum of the van der Waals radii of the S atoms (3.7 Å). At 110 K this distance is 3.4264 (4) Å (Dahaoui *et al.*, 1999). These interactions run perpendicular to the *c*-axis direction, and the S···S contact is approximately co-linear with the S—S covalent bond. Trends in the geometries of such interactions have been shown to be consistent with donation of a lone pair into an S—S-based σ^* molecular orbital (Dahaoui *et al.*, 1999).

3.2. The response of hexagonal L-cystine to pressure up to 3.7 GPa

Hexagonal L-cystine was found to be stable up to 6.4 GPa. However, no structural data could be extracted above 5.0 GPa, and even at this pressure the refined parameters are imprecise. Therefore only structural data to 3.7 GPa were used for comparison with the ambient pressure structure. The S—S distance appears to decrease from 2.043 (2) to 2.038 (5) Å, though this is not statistically significant. Other bond distances and angles were restrained during refinement to their ambient pressure values, and so no conclusions about their variation with pressure should be drawn from these data. Significant changes do occur in the torsion angles, however. The C—S—S—C torsion angle reduces from 75.20 (7)° at ambient pressure to 72.3 (4)° at 3.7 GPa, while the N1—C2—C3—O2 torsion angle (also referred to as NCαCO or ψ in macromolecular crystallography) also reduces from 166.12 (8)° to 164.1 (7)°.

3.2.1. Lattice parameters. The response of the lattice parameters of hexagonal L-cystine to pressure is anisotropic, with the principal component of the strain tensor acting in the *c*-axes direction. Between ambient pressure and 6.4 GPa the *c*-axis reduces in length by 6.8%; the reduction in the *a*-axis length is 4.4%. The volume change in the initial 0.4 GPa range is approximately 1.0%, while from 0.4 to 6.4 GPa the volume changes by approximately 2.8% every 1.0 GPa until the sample became polycrystalline.

Changes in unit-cell dimensions and volume as a function of pressure are plotted in Fig. 5. The strain induced within molecular systems by pressure is usually anisotropic, and in layered structures the greatest direction of strain is often observed to be normal to the layers. Such behaviour has been observed, for example, in the monoclinic and orthorhombic polymorphs of paracetamol (Boldyreva *et al.*, 2000, 2002) and is also observed in L-cystine, where the direction of greatest compressibility is normal to the glycine-like layers formed within the structure.

The bulk modulus (K_0), refined for a Birch–Murnaghan equation of state (Birch, 1947; Angel, 2004) to second order, is 29.1 (4) GPa. The data set used to calculate this quantity is admittedly rather limited, and the values of V_0, K' and K'' were fixed at 1424.3 Å^3, 4 and −0.1337 GPa^{-1}, respectively; the values of V_0 and K' did not change significantly from these values on refinement. Molecular solids typically have $K_0 <$ 30 GPa (Angel, 2004), and the value obtained for L-cystine-I is towards the high end of this range. Slebodnick *et al.* (2004) quote the following K_0 values which are useful for comparison: $Ru_3(CO)_{12}$ 6.6 GPa, NaCl 25 GPa, quartz 37 GPa, ceramics 50–300 GPa and diamond 440 GPa.

Table 2
Hydrogen-bonding parameters in hexagonal L-cystine.

Distances are in Å, of which only $D\cdots A$ distances are given (see *Experimental*).

	Pressure (GPa)				
	0	0.4	1.4	2.3	3.7
N1H4···O1^{i}					
N1···O1	2.792 (5)	2.777 (2)	2.732 (2)	2.693 (4)	2.643 (7)
N1H4···O2^{i}					
N1···O2	3.147 (5)	3.119 (2)	3.071 (3)	3.029 (3)	2.970 (7)
N1H5···O2^{ii}					
N1···O2	2.816 (4)	2.806 (3)	2.769 (3)	2.742 (4)	2.703 (8)
N1H6···O1^{iii}					
N1···O1	2.842 (4)	2.829 (5)	2.815 (5)	2.781 (8)	2.786 (14)
C1H1···O2^{i}					
C1···O2	3.259 (6)	3.235 (3)	3.190 (3)	3.153 (5)	3.124 (9)
C2H3···O1^{iv}					
C2···O1	3.499 (4)	3.480 (2)	3.407 (2)	3.355 (3)	3.285 (6)

Symmetry codes: (i) $x, -1+y, z$; (ii) $1+x, y, z$; (iii) $1+x-y, 2-y, -z$; (iv) $-1+x, -1+y, z$.

3.2.2. NH···O hydrogen bonds. Variation in hydrogen-bonding parameters between ambient and 3.7 GPa are given in Table 2. H atoms were placed in idealized positions during refinement, and so we quantify hydrogen bonding with increasing pressure by using hydrogen bond donor-to-acceptor (N···O) distances rather than H···O distances.

The most compressible of the NH···O hydrogen bonds was found to be the longer interaction in the bifurcated N1—H4···O1/O2 hydrogen bond. Between 0 and 3.7 GPa N1···O2 shortens from 3.147 (5) to 2.970 (7) Å at 3.7 GPa. The shorter of the hydrogen bonds, N1—H4···O1, also decreases in length from 2.792 (5) Å to 2.643 (7) Å. This head-to-tail hydrogen-bonding interaction is also observed in α-glycine and serine, but in these structures it is less compressible than observed in this study, shortening from 2.7703 (9) to 2.740 (7) Å in α-glycine at 6.2 GPa, and from 2.871 (3) to 2.775 (13) Å in serine at 4.8 GPa.

The other hydrogen bond formed within the glycine-like layers, N1—H5···O2, decreases in length from 2.816 (4) Å to 2.690 (18) Å. A search of the CSD reveals that there are no ambient pressure amino acid structures (out of 213 hits) with N—H···O interactions shorter than N1···O1 at 3.7 GPa, and only three amino acid structures shorter than N1···O2 at 3.7 GPa. The shortest interaction at ambient pressure [2.661 (2) Å] was observed in L-arginine L-glutamate trihydrate (DUSMAF; Suresh *et al.*, 1986).

The fourth hydrogen bond, N1—H6···O1, which interacts between the layers to form an $R_2^2(10)$ ring motif, decreases in

length from 2.842 (4) Å to 2.786 (14) Å at 3.7 GPa. The O···C contacts formed between the carboxyl groups across the rings are of a similar length at ambient pressure [3.243 (1) Å] to those observed in dipolar C═O···C═O contacts (2.92–3.32 Å), though the geometry does not match any of the common types identified by Allen *et al.* (1998). These contacts also shorten only modestly to 3.200 (14) Å at 3.7 GPa. For comparison, the sheared-parallel C═O···C═O contacts formed in acetone at 0 and 1.5 GPa are 3.587 (3) and 3.365 (2) Å in acetone-II (Allan *et al.*, 1999).

This is the least compressible of the head-to-tail NH···OOC interactions even though it is formed in the same direction as the most compressible unit-cell dimension, the *c*-axis.

3.2.3. CH···O hydrogen bonds. Within the glycine-like layers the compression of weak C—H···O interactions parallels the compression of the N—H···O interactions. The more compressible is C2—H3···O1, which shortens from C···O = 3.499 (4) Å to 3.285 (6) Å. This interaction runs approximately parallel to the N1—H5···O2 hydrogen bond. C1—H1···O2 (formed in the same direction as N1—H4···O1) shortens from 3.259 (6) Å to 3.124 (9) Å.

3.2.4. S···S interactions. The structure of L-cystine is notable for the formation of S···S contacts which are substantially shorter [3.444 (4) Å] than the sum of the van der Waals radii of the S atoms (3.6 Å; Bondi, 1964). Under pressure, this contact shortens to 3.263 (4) Å at 3.7 GPa. A search of the CSD reveals 19 entries containing a C(sp^3)—S—S—C(sp^3) fragment in which an S···S contact is observed

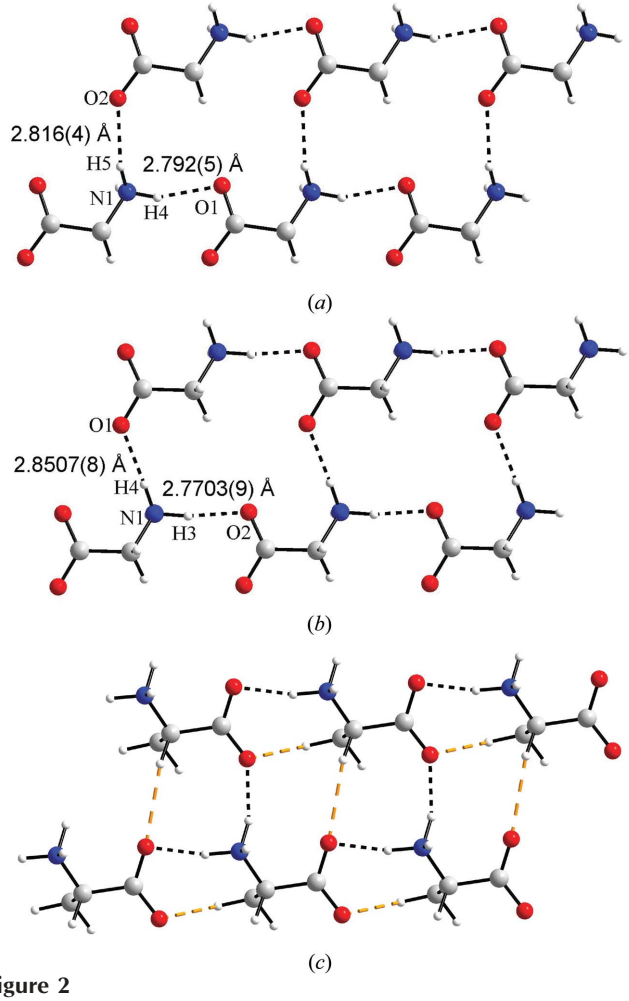

Figure 2
$R_4^4(16)$ ring motifs in (*a*) hexagonal L-cystine and (*b*) α-glycine, as viewed perpendicular to the *c*- and *b*-axes, respectively; the figures correspond to N···O distances in N—H···O hydrogen bonds. (*c*) $R_4^4(16)$ ring motifs created by interlaced CH···O and NH···O interactions in cystine as viewed perpendicular to the *c*-axis. The black dotted lines represent the ring motif as created by NH···O hydrogen bonds [*cf.* (*a*)], while the orange dotted lines show the interlaced ring motif as created by CH···O interactions. In (*a*) and (*c*) only the basic α-amino acid unit involved within the ring motif is shown for the sake of clarity. Colour scheme: C, grey; H, white; O, red; N, blue.

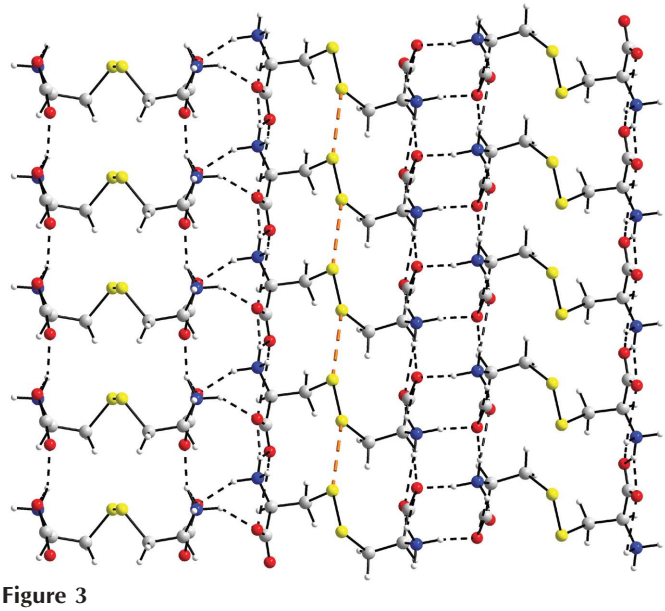

Figure 3
Hydrogen-bonded glycine-like double layers linked down the *c*-axis by disulfide bridges. This view is along **a**, with the *c*-axis running from left to right. The dashed black lines correspond to N···O hydrogen bonds; the dashed orange lines are S···S contacts. Sulfur is shown in yellow, but otherwise the colour scheme is as Fig. 2.

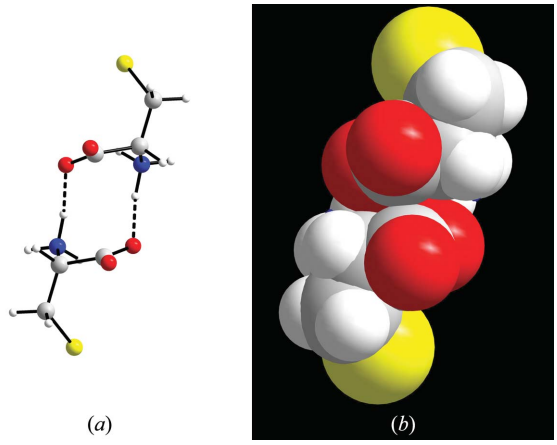

Figure 4
$R_2^2(10)$ ring motif as viewed perpendicular to the *c*-axis. (*a*) Standard ball-and-stick model; (*b*) space-filling model of (*a*) on the same scale. Half of each L-cystine molecule has been removed for clarity. Note the apparent lack of free space at the centre of the $R_2^2(10)$ ring.

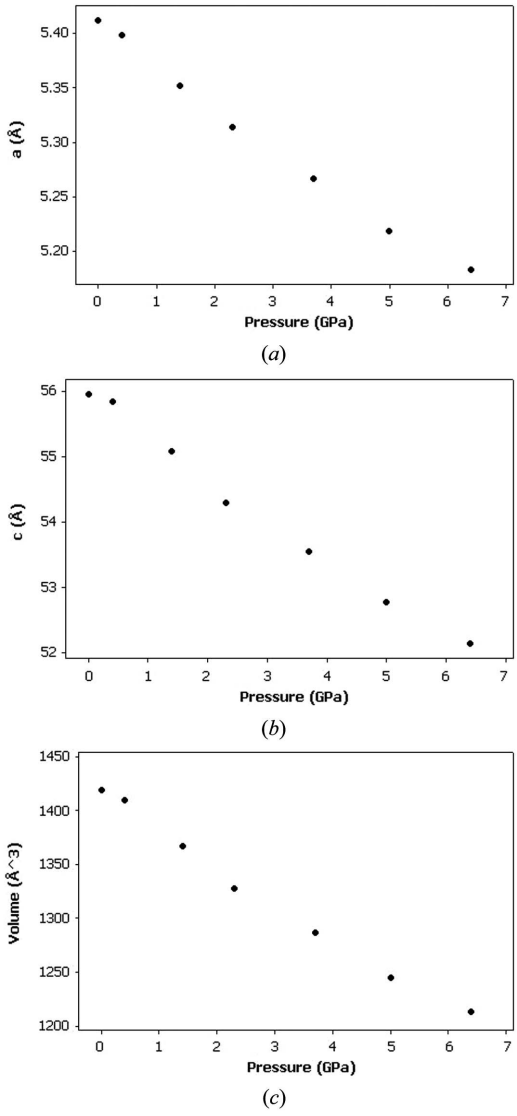

Figure 5
Variation of lattice parameters (a, c) (Å) and volume (Å^3) of hexagonal L-cystine as a function of pressure (GPa).

between 2.5 and 3.7 Å. All of these structures were determined at ambient pressure. The distribution is rather uniform in this distance range, but the shortest contact observed so far (refcode KOWMEO; Fujimura *et al.*, 1992) measures 3.31 Å. The application of pressure has therefore caused the S···S interaction to reduce in length close to the lower distance limit observed under ambient pressure conditions.

4. Discussion

4.1. Anisotropic compression of L-cystine

In pressure studies of α-glycine and L-serine-I we have ascribed trends in the relative compressibilities of C—H···O and N—H···O hydrogen bonds to the closing up of voids existing in the structure at ambient pressure. At pressure these voids contract with the shortening of N—H···O and C—H···O interactions. Similar conclusions on the importance of void closure were drawn in a study of $Ru_3(CO)_{12}$. Recent work by Blatov & Shevchenko (2003) makes it possible to analyse the sizes and distributions of voids in crystal structures using the Voronoi-Dirichlet formalism.

The environment of an atom in a crystal structure can be visualized using a Voronoi-Dirichlet polyhedron or VDP (Peresypkina & Blatov, 2000*a*,*b*). Voronoi-Dirichlet analysis is a method for partitioning space amongst points which occupy that space. A point is separated from a neighbouring point by a plane which bisects the vector between them. This construction is repeated for every pair of points to yield a subdivision of the space into cells which each contain one point. VDP analysis carried out using individual atoms to define the points leads to a molecular VDP, and these correspond to a complete partitioning of space in a crystal structure. Interatomic interactions occur at the points in the structure where faces of VDPs meet, whereas the topological definition of a void is a point at which the vertices of VDPs meet (Blatov & Shevchenko, 2003).

Fig. 6(*a*) shows the distribution of voids in the crystal structure of L-cystine at ambient pressure. The largest void conglomerate in the structure occurs in the vicinity of the S atoms; this is labelled 1 in Fig. 6(*a*). These voids straddle the short intermolecular S···S contact of 3.444 (4) Å, and the contraction of this distance to 3.263 (4) Å at 3.7 GPa is consistent with the orientation of the void conglomerates in this region of the structure.

Fig. 6(*b*) shows the distribution of voids in the region of the $R_4^4(16)$ rings formed in the glycine-like layers; this region is labeled 2 in Fig. 6(*a*). Fig. 7 illustrates the sizes of the voids in cystine at ambient pressure; the close correspondence between the positions of the voids in Fig. 7(*a*) and the largest void positions in Fig. 6(*b*) is readily apparent. On compression to 3.7 GPa the sizes of the voids in the $R_4^4(16)$ ring are reduced, leading to the observed shortening in the CH···O and NH···O hydrogen bonds which form within these layers. It is notable that the S···S interaction is approximately parallel to the N1—H4···O1 $C(5)$ chains, and the change of −0.18 Å in the former is reflected in the −0.15 Å change in the latter.

There is a collection of voids between the glycine-like sheets in the region labeled 3 in Fig. 6(*a*). Voids are less evident within the $R_2^2(10)$ ring motifs, which connect pairs of glycine-like layers, than in the $R_4^4(16)$ rings formed within the layers (see also Fig. 4). This may explain why the N1—H6···O1 hydrogen bond is the least compressible of the N—H···O interactions in the system. Larger voids do exist elsewhere in region 3 though, as shown in Fig. 6(*a*). There is a marked contraction of the void between the two O atoms labeled O2 in Fig. 8, with the O···O distance reducing from 3.643 (4) to 3.350 (15) Å, between ambient pressure and 3.7 GPa. The reduction of the N1—C2—C3—O2 torsion angle from 166.12 (8)° to 164.1 (7)° may also be associated with the void closure in this region of the structure. Overall the distance between the planes containing the C2 (or C_α) atoms in neighbouring glycine-like layers (labelled A in Fig. 9) reduces from 3.729 (2) Å at ambient pressure to 3.539 (21) Å at 3.7 GPa.

The final conglomerate of voids (4) occurs in the region formed by the $NH_3-CH-CH_2-S$ moieties. The C—S—S—C torsion angle reduces from 75.27 (18)° at ambient pressure to 72.3 (4)° at 3.7 GPa. Since the S—S bond is approximately perpendicular to the *c*-axis the conformational change reduces the height of the molecule in the *c*-direction, and the distance between the planes containing the C_α atoms either side of the disulfide bridges (labelled B in Fig. 9) reduces from 5.597 (2) Å at ambient pressure to 5.386 (22) Å at 3.7 GPa. The twisting action of the L-cystine molecules could be described as a molecular 'spring', whose action allows the compression of the structure along the *c*-axis direction.

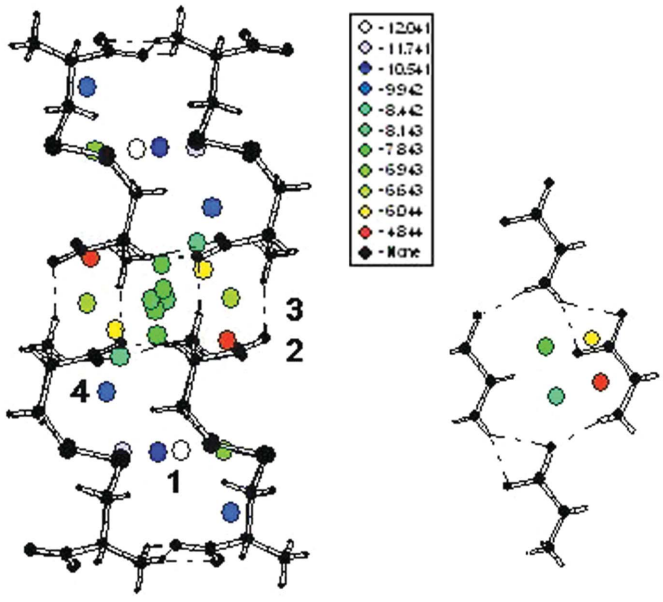

Figure 6
(*a*) The distribution of voids in cystine under ambient conditions, viewed with the *c*-axis vertical. The numbers 1–4 refer to regions of the structure, as discussed in the text. (*b*) Voids in the glycine-like $R_4^4(16)$ layers under ambient conditions. The colour scheme represents the volumes of the VDPs of the voids (in $Å^3$) as discussed by Blatov & Shevchenko (2003); the largest void is shown in white, voids then progressively decrease in volume from blue to red; precise values are given in the legend.

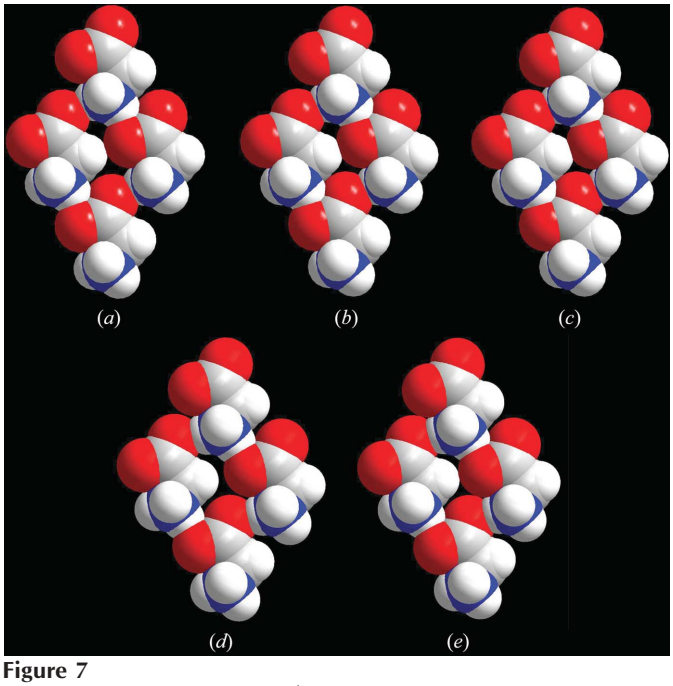

Figure 7
Space-filling plots showing $R_4^4(16)$ ring-motifs L-cystine at ambient temperature and pressure (*a*), 2.3 GPa (*b*) and 3.7 GPa (*c*), and α-glycine at ambient temperature and pressure (*d*) and at 2 GPa (*e*). Note the reduction in the sizes of the voids in the middle of the ring motifs with increasing pressure.

4.2. Comparison of compression in α-glycine and L-cystine

We have previously determined the crystal structure of α-glycine at 2.0 GPa (Dawson *et al.*, 2005), and in this paper we report the crystal structure of L-cystine at 2.3 GPa. Given the similarity in the layer structures of L-cystine and α-glycine it is interesting to compare the effect of pressures around 2 GPa

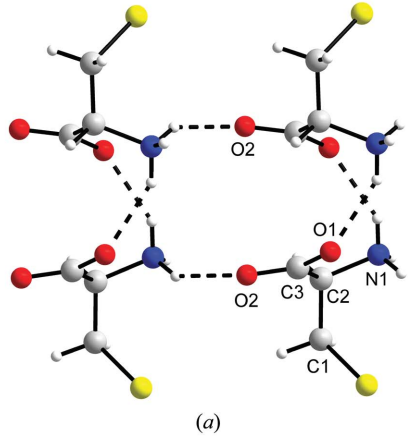

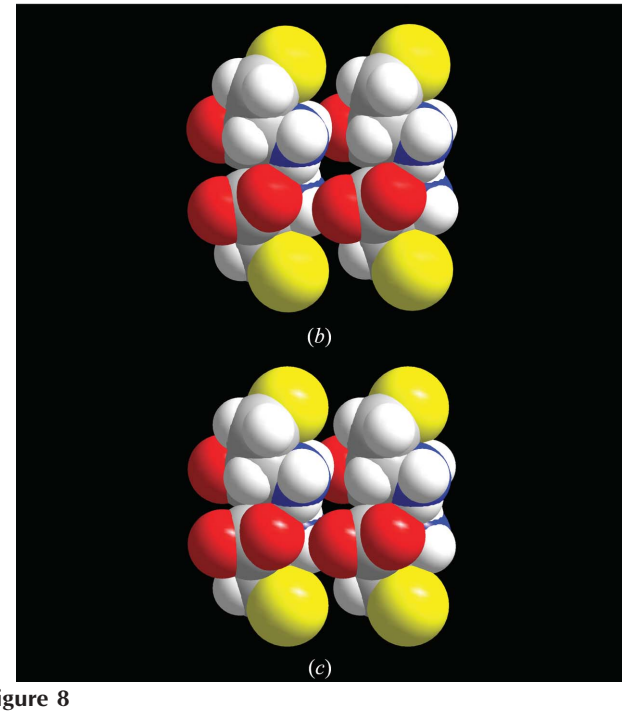

Figure 8
Voids formed between glycine-like layers at ambient pressure (*a* and *b*) and at 3.7 GPa (*c*). Note the reduction in the sizes of the voids in (*b*) and (*c*) with increasing pressure.

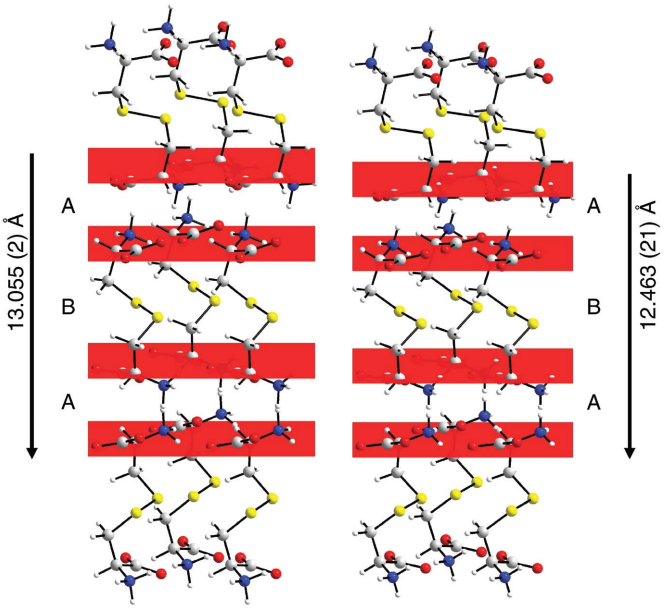

Figure 9
Ball-and-stick models of L-cystine at (*a*) ambient pressure and (*b*) 3.7 GPa as viewed down (01$\bar{2}$). The red planes are through the Cα atoms in each glycine-like layer running perpendicular to the *c*-axes of each plot. The overall compression of L-cystine caused *via* the 'twisting' of the molecules can be seen in compression between the layers (A), and between pairs of layers (B). The distance between layers A and B reduces from 3.729 (2) to 3.539 (21) Å, and 5.597 (2) to 5.386 (22) Å from ambient to 3.7 GPa, respectively. The distance between the first and last adjacent pairs of layers for both the ambient and 3.7 GPa data sets is shown.

on this part of the two crystal structures. Fig. 7 compares the voids in the two structures as a function of pressure.

α-Glycine is the more compressible of the two structures and at 2 GPa its unit-cell volume is 90% of its ambient pressure value; the corresponding figure of cystine is 93%. Comparison of Figs. 7(*a*) and 7(*d*) suggests that the voids in the centres of the $R_4^4(16)$ rings are slightly larger in α-glycine than in cystine, and this observation can be quantified by comparison of the respective areas of the *ac* and *ab* unit-cell faces in the two structures.[2] At ambient pressure these areas are 25.904 (2) Å^2 for glycine and 25.444 (3) Å^2 for cystine. At 2 GPa the areas are remarkably similar: 24.429 (8) Å^2 for glycine and 24.446 (1) Å^2 for cystine.

The overall similarity of the structures of the glycine-like layers is reflected in the similarity of the mean values of the principal components of the strain tensor which reside in the layers in both structures, *viz.* −0.03 for glycine and −0.02 for cystine. That the value for glycine is slightly higher than for cystine is presumably ascribable to the more efficient packing in cystine at ambient pressure.

Compression in the *ab* plane of cystine is constrained by the crystal symmetry to be isotropic, and this is reflected in the similar responses of the N1—H4···O1 and N1—H5···O2 hydrogen-bond distances to pressure (Table 2), which shorten by 0.10 and 0.08 Å, respectively. In α-glycine [which is monoclinic with the *b*-direction perpendicular to the view shown in Figs. 7(*d*) and 7(*e*)] the strain is markedly anisotropic. The largest strain component (−0.06) acts to close up the voids in the structure by forming a CH···O interaction as shown in Figs. 7(*d*) and 7(*e*). The N—H···O hydrogen bond which forms parallel to this C—H···O interaction shortens by 0.10 Å, whereas the other barely changes in length at all.

5. Conclusions

We have described the effect of pressure on the structure of hexagonal L-cystine at room temperature up to 3.7 GPa, with data on unit-cell dimensions reported up to 6.4 GPa. The structure can be described as being composed of pairs of glycine-like layers which lie in the *ab* plane. Each layer is composed of head-to-tail NH···OOC hydrogen bonds which combine to produce an $R_4^4(16)$ ring motif. Another NH···OOC hydrogen-bonding interaction then links the layers together in pairs *via* a $R_2^2(10)$ ring motif perpendicular to the *c*-axis. Paired layers then repeat down the *c*-axis separated by disulfide bridges about the 6_1 screw axes.

Under pressure, the structure undergoes anisotropic compression with the direction of greatest strain acting in the *c*-axis direction. This direction is normal to the glycine-like layers within the structure, which up to 3.7 GPa are pushed closer together along the *c*-axis direction. This compression occurs with the closing up of voids which are distributed along the *c*-direction (in regions 3 and 4 in Fig. 6). As this closure proceeds, two intramolecular torsion angles decrease, C1—S1—S1′—C1′ and N1—C2—C3—O2. Compression in the *ab* planes is constrained to be isotropic by symmetry and acts to decrease an already short S···S interaction and to close up voids within the $R_4^4(16)$ rings with a shortening of both N—H···O and C—H···O distances.

We thank the EPSRC and the University of Edinburgh for funding and the CCLRC for provision of synchrotron beam time. We also thank Professor R. J. Nelmes and Dr M. I. McMahon (both University of Edinburgh) for the use of some of their equipment at Daresbury SRS. We also thank Professor V. Blatov (Samara University, Russia) for his advice on the use of *TOPOS*.

[2] The unit-cell data for α-glycine at ambient pressure [2.0 GPa] are: monoclinic, a = 5.1047 (3) [4.9669 (9)], b = 11.9720 (14) [11.459 (4)], c = 5.4631 (3) [5.4231 (12)] Å, β = 111.740 (5)° [114.916 (15)°]. All data were measured at room temperature. References: Boldyreva *et al.* (2003) and Dawson *et al.* (2005).

References

Allan, D. R., Clark, S. J., Ibberson, R. M., Parsons, S., Pulham, C. R. & Sawyer, L. (1999). *Chem Commun.* pp. 751–752.
Allan, D. R., Parsons, S. & Teat, S. J. (2001). *J. Synchrotron Rad.* **8**, 10–17.
Allen, F. H. (2002). *Acta Cryst.* B**58**, 380–388.
Allen, F. H., Baalham, C. A., Lommerse, J. P. M. & Raithby, P. R. (1998). *Acta Cryst.* B**54**, 320–329.
Allen, F. H. & Motherwell, W. D. S. (2002). *Acta Cryst.* B**58**, 407–422.
Angel, R. (2002*a*). *Rev. Mineral. Geochem.* **41**, 35–59.
Angel, R. (2002*b*). *EOSFIT*. Version 5.2. Virginia Tech., Blackburg, VA, USA.

Angel, R. (2004). *High Pressure Crystallography, NATO Science Series II*, edited by A. Katrusiak and P. McMillan, pp 21–36. Dordrecht: Kluwer.
Berman, H. M., Westbrook, J., Feng, Z., Gilliland, G., Bhat, T. N., Weissig, H., Shindyalov, I. N. & Bourne, P. E. (2000). *Nucl. Acid Res.* **28**, 235–242.
Bernstein, J., Davis, R. E., Shimoni, L. & Chang, N.-L. (1995). *Angew. Chem. Int. Ed. Engl.* **34**, 1555–1573.
Betteridge, P. W., Carruthers, J. R., Cooper, R. I., Prout, K. & Watkin, D. J. (2003). *J. Appl. Cryst.* **36**, 1487.
Bhattacharaya, R., Pal, D. & Chakrabarti, P. (2004). *Prot. Eng. Des. Select.* **17**, 795, 808.
Birch, F. (1947). *Phys. Rev.* **71**, 809–824.
Blatov, V. A. & Shevchenko, A. P. (2003). *Acta Cryst. A***59**, 34–44.
Blatov, V. A., Shevchenko, A. P. & Serezhkin, V. N. (2000). *J. Appl. Cryst.* **33**, 1193.
Boldyreva, E. V. (2004*a*). *J. Mol. Struct.* **700**, 151–155.
Boldyreva, E. V. (2004*b*). *Cryst. Eng.* **6**, 235–254.
Boldyreva, E. V., Ahsbahs, H. & Weber, H.-P. (2003). *Z. Kristallogr.* **218**, 231–236.
Boldyreva, E. V., Shakhtshneider, T. P., Ahsbahs, H., Sowa, H. & Uchtmann, H. (2002). *J. Therm. Anal. Calorimetry*, **68**, 437–452.
Boldyreva, E. V., Shakhtshneider, T. P., Vasilchenko, M. A., Ahsbahs, H. & Uchtmann, H. (2000). *Acta Cryst.* B**56**, 299–309.
Bondi, A. (1964). *J. Phys. Chem.* **68**, 441–451.
Bruker-AXS (2003). *SAINT*. Version 7. Bruker-AXS, Madison, Wisconsin, USA.
Bruno, I. J., Cole, J. C., Edgington, P. R., Kessler, M., Macrae, C. F., McCabe, P., Pearson, J. & Taylor, R. (2002). *Acta Cryst.* B**58**, 389–397.
Cernik, R. J., Clegg, W., Catlow, C. R. A., Bushnell-Wye, G., Flaherty, J. V., Greaves, G. N., Burrows, I., Taylor, D. J., Teat, S. J. & Hamichi, M. (1997). *J. Synchrotron Rad.* **4**, 279–286.
Chaney, M. O. & Steinrauf, L. K. (1974). *Acta Cryst.* B**30**, 711–716.
Crystal Impact (2004). *DIAMOND*. Version 3.0. Crystal Impact GbR, Postfach 1251, 53002 Bonn, Germany (http://www.crystalimpact.com/diamond).
Dahaoui, S., Pichon-Pesme, V., Howard, J. A. K. & Lecomte, C. (1999). *J. Phys. Chem. A*, **103**, 6240–6250.
Dawson, A., Allan, D. R., Belmonte, S. A., Clark, S. J., David, W. I. F., McGregor, P. A., Parsons, S., Pulham, C. R. & Sawyer, L. (2005). *Cryst. Growth Des.* **5**, 1415–1427.
Dawson, A., Allan, D. R., Clark, S. J., Parsons, S. & Ruf, M. (2004). *J. Appl. Cryst.* **37**, 410–416.
Derewenda, Z. S., Lee, L. & Derewenda, U. (1995). *J. Mol. Biol.* **252**, 248–262.
Desiraju, G. R. & Steiner, T. (1999). *The Weak Hydrogen Bond, IUCr Monographs on Crystallography No. 9.* Oxford University Press.
Farrugia, L. J. (1999). *J. Appl. Cryst.* **32**, 837–838.
Fujimura, K., Ito, S., Suhara, H. & Kawashima, Y. (1992). *J. Chem. Res.* pp. 88–89.
Görbitz, C. H. (1990). *Acta Chem. Scand.* **44**, 584–590.
Jeffrey, G. A. & Maluszynska, H. (1982). *Int. J. Biol. Macromol.* **4**, 173–185.
Merrill, L. & Bassett, W. A. (1974). *Rev. Sci. Instrum.* **45**, 290–294.
Moggach, S. A., Allan, D. R., Morrison, C. A., Parsons, S. & Sawyer, L. (2005). *Acta Cryst.* B**61**, 58–68.
Morris, A. L., MacArthur, M. W., Hutchinson, E. G. & Thornton, J. M. (1992). *Proteins: Struct. Funct. Genet.* **12**, 345–364.
Oswald, I. D. H., Allan, D. R., Day, G. M., Motherwell, W. S. D. & Parsons, S. (2005). *Cryst. Growth Des.* **5**. 1055–1071.
Oswald, I. D. H., Allan, D. R., Motherwell, W. S. D. & Parsons, S. (2005). *Acta Cryst.* B**61**, 69–79.
Oughton, B. M. & Harrison, P. M. (1959). *Acta Cryst.* **12**, 396–404.
Parsons, S. (2004). *SHADE. Program for Empirical Absorption Corrections to High Pressure Data.* The University of Edinburgh, Scotland.
Peresypkina, E. V. & Blatov, V. A. (2000*a*). *Acta Cryst.* B**56**, 501–511.
Peresypkina, E. V. & Blatov, V. A. (2000*b*). *Acta Cryst.* B**56**, 1035–1045.
Piermarini, G. J., Block, S., Barnett, J. D. & Forman, R. A. (1975). *J. Appl. Phys.* **46**, 2774–2780.
Richardson, J. S. (1981). *Adv. Prot. Chem.* **34**, 167–339.
Sheldrick, G. M. (1997). *XP*. University of Göttingen, Germany.
Sheldrick, G. M. (2004). *SADABS*. University of Göttingen, Germany.
Slebodnick, C., Zhao, J., Angel, R., Hanson, B. E., Song, Y., Liu, Z. & Hemley, R. J. (2004). *Inorg. Chem.* **43**, 5245–5252.
Spek, A. L. (2004). *PLATON – A Multipurpose Crystallographic Tool.* Utrecht University, The Netherlands.
Suresh, C. G., Ramaswamy, J. & Vijayan, M. (1986). *Acta Cryst.* B**42**, 473–478.
Thornton, J. M. (1981). *J. Mol. Biol.* **151**, 261–287.
Watkin, D. J., Pearce, L. & Prout, C. K. (1993). *CAMERON – A Molecular Graphics Package.* Chemical Crystallography Laboratory, University of Oxford, England.
Wunschel, M., Dinnebier, R. E., Carlson, S., Bernatowicz, P. & van Smaalen, S. (2003). *Acta Cryst.* B**59**, 60–71.